Visualization of a radical B[subscript 12] enzyme with its G-protein chaperone

Citation: Jost, Marco, Valentin Cracan, Paul A. Hubbard, Ruma Banerjee, and Catherine L. Drennan. "Visualization of a Radical B[subscript 12] Enzyme with Its G-Protein Chaperone." Proc Natl Acad Sci USA 112, no. 8 (February 9, 2015): 2419–2424.

As Published: http://dx.doi.org/10.1073/pnas.1419582112

Publisher: National Academy of Sciences (U.S.)

Persistent URL: http://hdl.handle.net/1721.1/98024

Version: Final published version: final published article, as it appeared in a journal, conference proceedings, or other formally published context

Visualization of a radical B_{12} enzyme with its G-protein chaperone

Marco Jost[a], Valentin Cracan[b,1], Paul A. Hubbard[a,2], Ruma Banerjee[b], and Catherine L. Drennan[a,c,d,3]

[a]Department of Chemistry and [c]Department of Biology, [d]Howard Hughes Medical Institute, Massachusetts Institute of Technology, Cambridge, MA 02139; and [b]Department of Biological Chemistry, University of Michigan, Ann Arbor, MI 48109-0600

Edited by Markus W. Ribbe, University of California, Irvine, CA, and accepted by the Editorial Board January 21, 2015 (received for review October 14, 2014)

G-protein metallochaperones ensure fidelity during cofactor assembly for a variety of metalloproteins, including adenosylcobalamin (AdoCbl)-dependent methylmalonyl-CoA mutase and hydrogenase, and thus have both medical and biofuel development applications. Here, we present crystal structures of IcmF, a natural fusion protein of AdoCbl-dependent isobutyryl-CoA mutase and its corresponding G-protein chaperone, which reveal the molecular architecture of a G-protein metallochaperone in complex with its target protein. These structures show that conserved G-protein elements become ordered upon target protein association, creating the molecular pathways that both sense and report on the cofactor loading state. Structures determined of both apo- and holo-forms of IcmF depict both open and closed enzyme states, in which the cofactor-binding domain is alternatively positioned for cofactor loading and for catalysis. Notably, the G protein moves as a unit with the cofactor-binding domain, providing a visualization of how a chaperone assists in the sequestering of a precious cofactor inside an enzyme active site.

metallocofactor delivery | vitamin B_{12} | metallochaperone | G protein | crystallography

Metallocofactors are ubiquitous in biology and essential for many cellular processes. Their use comes at a price, however, because metallocofactors are expensive to biosynthesize and transport, can have associated toxicity, and must be correctly assembled into their target enzyme for activity. To address these challenges, nature often employs protein metallochaperones. Chaperone-assisted cofactor delivery limits cellular dilution, minimizes inadvertent reactivity associated with the free cofactor, and ensures proper enzyme assembly (1–3). The importance of metallocofactor trafficking is underscored by the manifestation of diseases when mutations affect trafficking proteins. One important group of metallochaperones comprises the small guanine nucleotide-binding proteins (G proteins) belonging to the SIMIBI class (after signal recognition particle, MinD, and BioD) of P-loop NTPases (4). The human G-protein chaperone, MMAA (methylmalonic aciduria type A protein, mitochondrial; gene product of *cbl*A), is involved in the assembly of adenosylcobalamin (AdoCbl, coenzyme B_{12})-dependent methylmalonyl-CoA mutase (MCM) (5, 6). Mutations in MMAA and MCM result in methylmalonic aciduria, a genetically inherited metabolic disease that is devastating in newborns and infants (7). Bacterial homologs of MMAA are involved in assembly of other metalloproteins and include HypB for hydrogenase (8) and UreG for urease (9). These G-protein chaperones bind to their target proteins and then use their GTP hydrolase (GTPase) activity to assist maturation of the target with high specificity (10–12). The mechanisms by which these essential chaperones perform their functions, however, are not well established, in large part because of the absence of structural information on their complexes with target proteins.

An extensively studied member of the G-protein chaperones is MeaB[12–14], a bacterial ortholog of MMAA. Its target MCM requires AdoCbl to catalyze the radical-mediated 1,2-rearrangement of methylmalonyl-CoA (CoA) to succinyl-CoA (Fig. S1*A*) (13), an essential step in the degradation of odd-chain fatty acids, cholesterol, and branched amino acids. In this reaction and those of related isomerases, AdoCbl serves as a radical reservoir, reversibly generating the working 5′-deoxyadenosyl radical via homolytic cleavage of its cobalt–carbon bond (13–15). It is critically important for these isomerases to be loaded with AdoCbl and not any other cofactor derivative, which would yield inactive enzyme. MeaB performs this gating function for MCM and uses its GTPase activity to enable cofactor delivery (12) from the adenosyltransferase that synthesizes AdoCbl (16, 17). MeaB additionally remains associated with MCM during turnover and reduces the rate of oxidative inactivation (18). Notably, MeaB is structurally and mechanistically distinct from the ATP-dependent chaperones for AdoCbl-dependent eliminating enzymes, such as diol dehydratase: these chaperones, also termed reactivases, bind to inactivated enzymes and use their ATPase activity to eject damaged cofactor but do not affect AdoCbl delivery (19). An ortholog of MeaB, MeaI, is found fused to isobutyryl-CoA mutase. Termed IcmF (20), the fusion protein exhibits both GTPase activity and AdoCbl-dependent carbon skeleton isomerase activity, interconverting isobutyryl-CoA and *n*-butyryl-CoA, as well as pivalyl-CoA and isovaleryl-CoA (Fig. S1 *B* and *C*) (20, 21). The latter activity is newly discovered and may have relevance to the biodegradation of branched compounds (22).

Significance

Metalloproteins are ubiquitous, accounting for about 30–50% of all proteins. Their functions are wide-ranging, but metalloproteins are frequently used to carry out challenging molecular transformations. Metalloprotein reactivity comes at a price, however, often requiring specialized molecular machinery for holoenzyme assembly. G-protein metallochaperones are an important part of this assembly apparatus, but an understanding of their molecular mechanisms has been hindered by a lack of structural data. Here, we describe crystal structures of a G-protein metallochaperone together with a target enzyme, in this case an adenosylcobalamin-dependent radical enzyme, thereby providing a visualization of the molecular architecture of the G-protein:target enzyme complex.

Author contributions: M.J., V.C., R.B., and C.L.D. designed research; M.J. and V.C. performed research; V.C., P.A.H., and R.B. contributed new reagents/analytic tools; M.J. and C.L.D. analyzed data; and M.J. and C.L.D. wrote the paper.

The authors declare no conflict of interest.

This article is a PNAS Direct Submission. M.W.R. is a Guest Editor invited by the Editorial Board.

Data deposition: The atomic coordinates have been deposited in the Protein Data Bank, www.pdb.org [PDB ID codes 4XC6 (holo-IcmF GDP), 4XC7 (apo-IcmF) and 4XC8 (apo-IcmF GDP)].

[1]Present address: Department of Molecular Biology, Howard Hughes Medical Institute, Massachusetts General Hospital, Harvard Medical School, Boston, MA 02114.

[2]Present address: Department of Biomedical Sciences, Cedars-Sinai Medical Center, Los Angeles, CA 90048.

[3]To whom correspondence should be addressed. Email: cdrennan@mit.edu.

This article contains supporting information online at www.pnas.org/lookup/suppl/doi:10.1073/pnas.1419582112/-/DCSupplemental.

Herein, we present the crystal structure of IcmF from *Cupriavidus metallidurans* containing bound AdoCbl and GDP•Mg^{2+}, providing what is, to our knowledge, the first visualization of the juxtaposition of a G-protein chaperone and its target AdoCbl-dependent mutase. In addition, the crystal structure of IcmF in the absence of cofactors reveals the conformational changes required for cofactor loading.

Results

Conserved GTPase Elements Are Involved in G-Protein:Mutase Complex Formation. To visualize the molecular architecture of a G-protein:mutase complex, we determined the crystal structure of *C. metallidurans* IcmF with bound AdoCbl and GDP•Mg^{2+} (holo-IcmF•GDP) to 3.35 Å resolution (Fig. 1, Fig. S2, and Table S1). Each protomer of the IcmF dimer consists of four functional domains: an N-terminal cobalamin (Cbl)-binding Rossmann-fold domain (residues 21–157), a G-domain (residues 169–417), a structured linker region involved in dimer formation (residues 418–579), and a C-terminal acyl-CoA substrate-binding domain with an $(\alpha/\beta)_8$ triose phosphate isomerase (TIM) barrel fold (residues 580–1093) (Fig. 1 *A*–*C*).

Both the Cbl- and substrate-binding domains of IcmF share high similarity to other known AdoCbl-dependent mutases, such as MCM and glutamate mutase (Fig. 1 *B* and *D*, Fig. S3 *A*–*C*, and Table S2) (23–26). As with these other enzymes, AdoCbl is bound to a Rossmann-fold domain in a "base-off/His-on" conformation with a His (His39) serving as the lower axial ligand to the cobalt (Fig. S3 *D* and *E*) and the 5′-deoxyadenosyl group (5′-dAdo) positioned in the active site cavity on the C-terminal face of the substrate-binding TIM barrel. Acyl-CoA substrates are known to access the AdoCbl cofactor by threading through the TIM barrel (Fig. S3*F*), which can open and close (23, 27). Finally, the dimer architecture of IcmF is similar to other AdoCbl-dependent mutases, with substantial parts of the dimer interface formed by the substrate-binding domains (Fig. S3 *G*–*I*). The linker region of IcmF, which is not conserved, additionally stabilizes the dimeric arrangement of the subunits.

Remarkably, the two G-domains of an IcmF dimer are located on opposite ends and do not share an interface (Fig. 1*A*), in contrast to all other G-protein metallochaperones characterized to date, which are dimers (28–31). Apart from this difference, the G-domain exhibits high structural similarity to other G-protein chaperones with a central seven-stranded β-sheet, which is flanked by α-helices on both sides (Fig. 1 *C* and *E* and Table S2) (29, 30), housing the signature G-protein motifs (Fig. 2*A*). The catalytically essential Mg^{2+} is coordinated by the side-chains of Ser223, Asp262, and Glu310 and by a β-phosphate oxygen of GDP (Fig. 2*A*). Asp249 is in proximity to the Mg^{2+}-binding site and seems ideally positioned to activate a water molecule for GTP hydrolysis, as predicted previously based on homology to HypB (32). Arg265, which was disordered in structures of MeaB alone, interacts with the phosphate groups of the bound GDP and could help stabilize the negative charge that builds up during GTP hydrolysis, thus playing the role of a *cis*-acting Arg finger.

This conserved nucleotide-binding site is located directly at the interface of the G-domain and the mutase substrate-binding domain (Fig. 1*F*), burying 667 $Å^2$ and 626 $Å^2$ on the G-domain and the substrate-binding domain, respectively. The substrate-binding domain contributes two hydrogen bonds to the GDP ribose, from the side-chain of Asn1092 and the backbone carbonyl of Glu973 (Fig. 2*B*). Glu973 is also involved in salt bridges with base specificity loop residues Arg361 and Lys358. Interestingly, Glu973 immediately precedes a long α-helix that spans the width of the TIM barrel and interacts with the Cbl-binding domain, thus connecting the nucleotide binding site with both mutase domains (Fig. 2*B*). Two other residues of the substrate-binding domain, Arg1091 and Asn1092, form hydrogen bonds across the interface via their backbone atoms to the side-chain

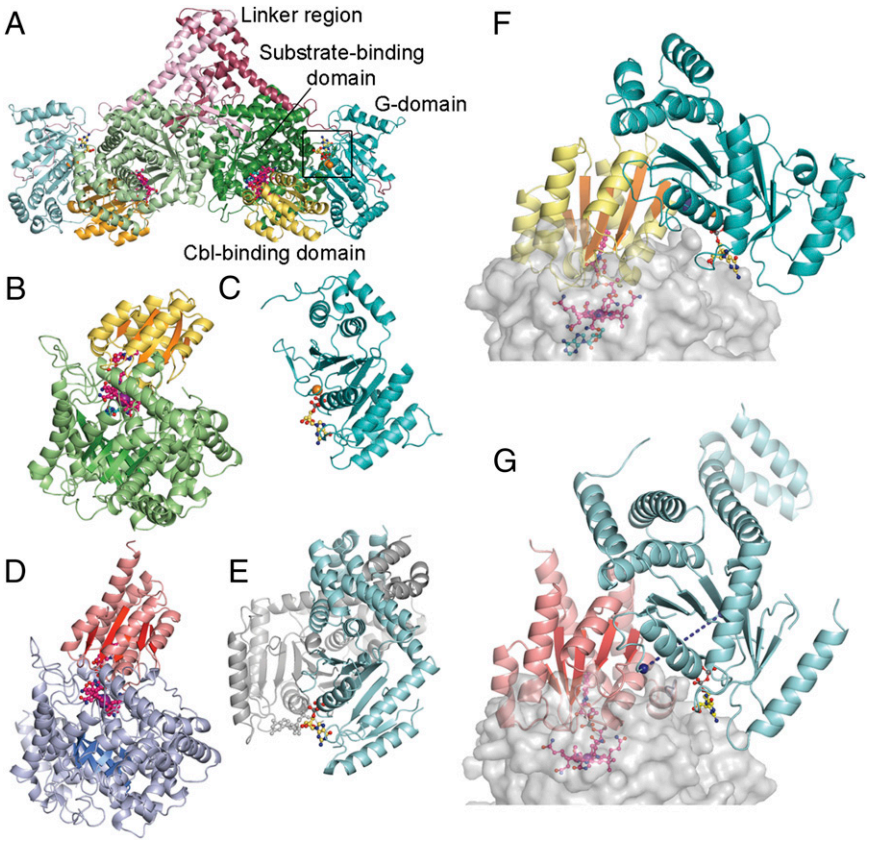

Fig. 1. Crystal structure of IcmF and comparison with MCM/MMAA. (*A*) Dimeric IcmF in ribbon depiction, colored by domain with one chain lighter than the other: yellow (Cbl-domains), cyan (G-domains), green (substrate-binding domains), pink/red (structured linker regions). AdoCbl shown in ball-and-stick with Cbl carbon in pink, 5′-dAdo carbon in cyan, cobalt in purple; GDP•Mg^{2+} in ball-and-stick with carbon in yellow, Mg^{2+} in orange. Boxed region shown in more detail in Fig. 2*A*. (*B* and *C*) IcmF protomer in a different orientation, with (*B*) mutase domains shown slightly separated from (*C*) the G-domain to emphasize shape complementarity. The second IcmF protomer and linker regions are not shown for clarity. (*D*) Human MCM protomer [PDB ID code 2XIQ (33)] and (*E*) dimeric MMAA [PDB ID code 2WWW (33)], shown in the same orientation as the corresponding IcmF domains in (*B*) and (*C*). MCM is colored in blue (substrate-binding domain) and red (Cbl-binding domain). The second MCM protomer is not shown for clarity. The MMAA protomers are shown in cyan and gray. MCM-bound Cbl and MMAA-bound GDP are shown as in *A*. (*F*) Close-up of IcmF domain interactions, with G- and Cbl-domains shown as in *A* and the substrate-binding domain in surface representation. (*G*) Structure-based docking model of the human MCM:MMAA complex, generated by superimposition of human MCM [PDB ID code 2XIQ (33)] and MMAA [PDB ID code 2WWW (33)] structures onto IcmF and oriented as in *F*. MCM shown with substrate-binding domain in surface representation and Cbl-domain in red, MMAA shown in cyan, Cbl and GDP shown as in *A*. Switch I of MMAA is disordered, locations of the chain breaks are indicated by spheres and connected by dashed lines.

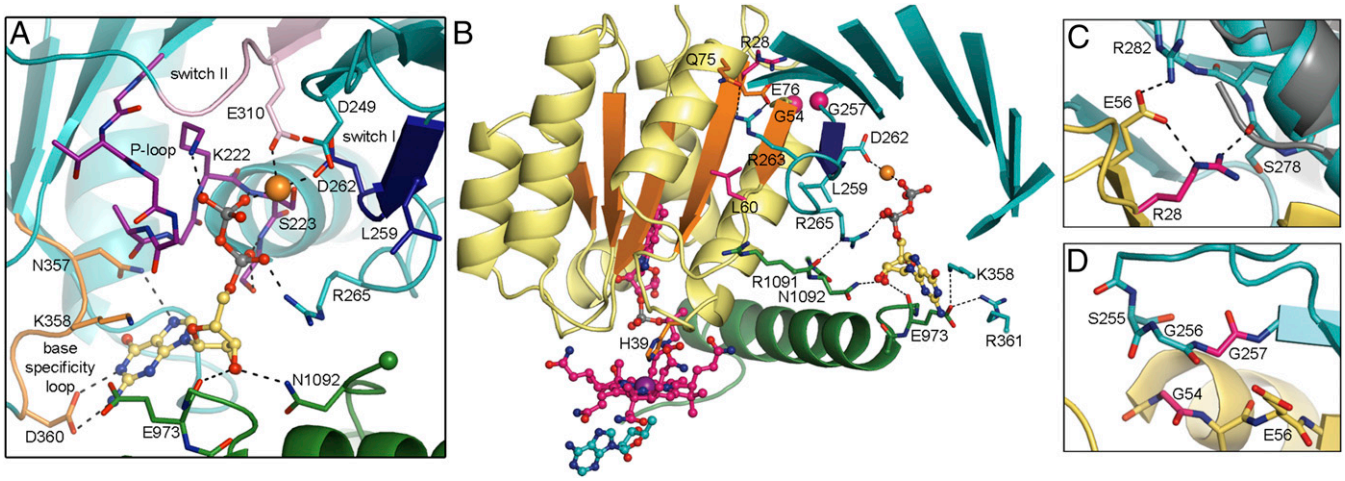

Fig. 2. Molecular interactions within and between IcmF domains. (*A*) IcmF GTPase active site with signature G-protein elements highlighted: Mg^{2+}-binding P-loop or Walker A motif (purple); switch I (dark blue), which is conformationally responsive to the GTPase cycle; switch II or Walker B motif (pink), which also undergoes conformational changes; and base specificity loop (orange) with the sequence NKxD that confers specificity to guanosine nucleotides. GDP•Mg^{2+} shown with carbon in yellow, Mg^{2+} in orange. Hydrogen bonds and coordination bonds are indicated by dashed black lines. Water molecules may additionally coordinate the Mg^{2+}, but are not visible in this structure because of its modest resolution. (*B*) Close-up view of the interactions between selected parts of the G-domain (cyan) and mutase Cbl- (yellow, orange) and substrate-binding domains (green), oriented as Fig. 1*F*. AdoCbl shown with Cbl carbon in pink, 5′-dAdo carbon in cyan, cobalt in purple. Switch I shown in dark blue. Interactions between G-domain and mutase domains are shown as black dashed lines, with residues shown as sticks with carbons colored by domains. Pathogenic mutations in MCM:MMAA, which have been mapped onto IcmF, are highlighted in pink (R28, G54, L60, G257). (*C* and *D*) Close-up view of mapped pathogenic mutations; see Fig. S4*B* for location in overall structure. IcmF, colored as in *B*, is superimposed with MMAA in gray. Highlighted pathogenic mutations are (*C*) Arg28 (MCM Arg616) as well as (*D*) Gly54 (MCM Gly642) and Gly257 (MMAA Gly188), shown in pink. In *D*, the corresponding region in MMAA is disordered and not shown.

of Arg265, which is likely involved in GTP hydrolysis as described above (Fig. 2*B*). It is notable how much of the G-protein:substrate-binding domain interface is comprised of residues from each domain that directly or indirectly contact GDP.

The interface between the G-domain and the Cbl-binding domain buries 969 Å^2 and 943 Å^2, respectively. Residues 258–261 of the G-domain, which were disordered in the structures of MeaB (29) and MMAA (33), form a short β-strand (Fig. 2*B*, dark blue) that hydrogen bonds to the outermost β-strand of the Cbl-binding domain (Fig. 2*B*, orange), creating an extended β-sheet. Interestingly, this domain-linking β-strand contains part of the GTPase switch I motif (Leu259) (Fig. 2 *A* and *B*) known to undergo conformational changes during the GTPase cycle. There are a number of interactions made between residues in or near switch I that connect the GDP•Mg^{2+}-binding site in the G-domain to the Cbl-domain. In particular, Asp262 of switch I and downstream Arg265 resemble a C-clamp, pointing toward and interacting with Mg^{2+} and GDP, respectively (Fig. 2*B*), whereas Arg263 points in the opposite direction and directly contacts the Cbl-domain via a bifurcated interaction with Gln75 and Glu76. Gln75, Glu76, Leu259, Asp262, Arg263, and Arg265 are all fully conserved in IcmF sequences (20).

Insights into MCM:G-Protein Complexes and Methylmalonic Aciduria from the IcmF Structure. Given the high structural similarity between the IcmF domains and the homologous domains of MCM and MMAA/MeaB, the IcmF crystal structure allows us to predict the architectures of MCM:G-protein chaperone complexes by 3D structural alignments. These structure-based docking models place MCM and the G proteins in the same relative positions as in IcmF, with complementary surfaces and no major clashes (Fig. 1*G*, and Figs. S4 and S5). In the modeled MCM:G-protein complexes (with MMAA or MeaB), GDP resides at the interface of the MCM substrate-binding domains and the G protein, where it can make similar interactions (Fig. S4 *A* and *B*). At least 10 residues that contribute to the interface between the IcmF Cbl-binding and G-domains are conserved in MCMs and their G proteins (Fig. S6), including the switch I motif and the interface-forming β-strand in the G protein.

Interestingly, a number of residues in MCM and MMAA that are associated with methylmalonic aciduria, map to this predicted interface. These residues include the MCM mutations R616C (R28 in IcmF) and G642R (G54 in IcmF), and G188R in MMAA (G257 in IcmF) (Fig. 2 *B–D* and Table S3). We expect all three of these mutations to substantially alter the MCM/MMAA interface: the MCM R616C mutation would disrupt several hydrogen bonds, whereas the MCM G642R or MMAA G188R mutations would introduce severe clashes. Similarly, two other disease-causing mutations, F573S and G648D, map to IcmF residues G1086 and L60, respectively. Both these residues are located at the mutase:G-protein interface in IcmF (Fig. S4 *D* and *E*).

Asymmetry Within the Holo-IcmF•GDP Structure Highlights Subunit Flexibility. Comparison of the two protomers of the holo-IcmF•GDP dimer reveals a displacement of the Cbl- and G-domains in one chain (B) relative to the other chain (A), leading to an ∼850 Å^2 difference in buried surface area and an 8 Å shift of the Cbl cofactor (Fig. 3*A* and Fig. S7*A*). Whereas the interactions between the Cbl and its binding domain are unchanged, almost all interactions between the Cbl and the substrate-binding domain are lost in chain B, with reduction of the buried surface area from 839 Å^2 to 159 Å^2 and concomitant loss of 5′-dAdo. Although the Cbl-binding domain is farther from the substrate-binding domain in chain B, parts of the G-domain are closer to the substrate-binding domain, increasing the interface between the latter two domains from 646 Å^2 to 768 Å^2. A difference distance matrix plot (34) demonstrates that the Cbl- and the G-domains move as a single rigid body that is best described as a swinging motion around a hinge centered at the nucleotide-binding site of the G-domain (Fig. 3*A* and Figs. S7*B* and S8). Given its location at the hinge, the guanosine nucleotide moves by only ∼3 Å, whereas the Cbl, which is far from the hinge, is displaced by a larger distance of ∼8 Å.

Inspection of crystal packing suggests that the chain B Cbl-binding domain is held in this extended position by lattice

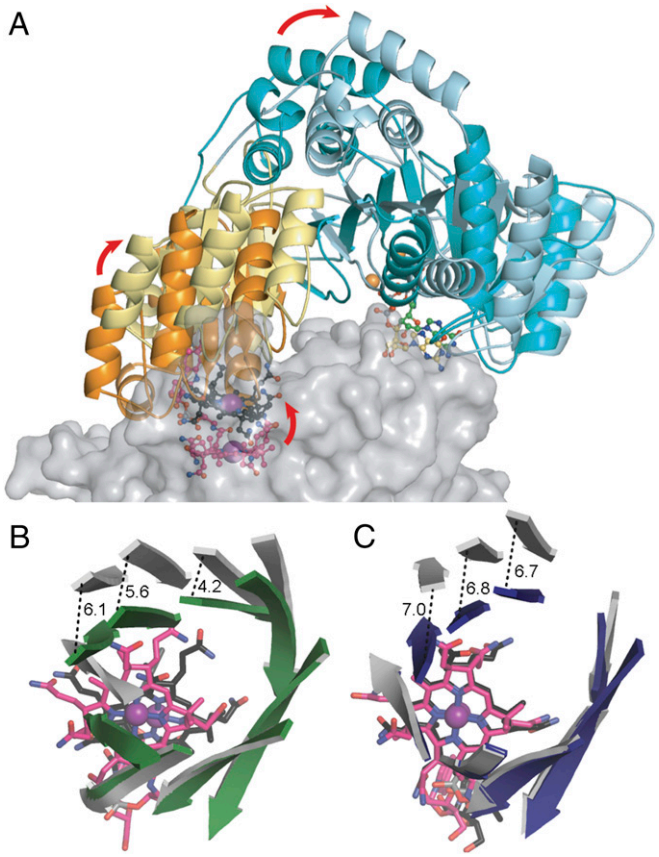

Fig. 3. Conformational movements in IcmF. (*A*) Differential positioning of the Cbl-domain and G-domain of holo-IcmF•GDP in chain A (cyan/orange) compared with chain B (light blue/yellow) when superimposed by their substrate-binding domains (gray surfaces). Cbl is shown in pink (chain A) and black (chain B), and GDP in yellow (chain A) and green (chain B). Mg^{2+} is shown as an orange sphere. 5′-dAdo not shown for clarity. (*B*) Superposition of the TIM barrel β-strands of holo-IcmF•GDP chains A (dark green) and B (gray). Cbl colored as in *A* and distances between corresponding C_α-atoms in Å. (*C*) Superposition of the TIM barrel β-strands of substrate-bound (dark blue) and substrate-free (gray) MCM [PDB ID codes 4REQ (35) and 2REQ (27), respectively]. Cbl is shown in pink (substrate-bound) and black (substrate-free).

contacts, whereas chain A makes fewer lattice contacts and is thus free to pack tightly against its substrate-binding domain (Fig. S7 *C* and *D*). Chain A represents an active state of the enzyme, with AdoCbl positioned in the barrel ready for catalysis, whereas chain B represents an inactive state with a cleaved Cbl cofactor positioned out of the active site.

The substrate-binding domains of the holo-IcmF•GDP dimer also exhibit structural differences (Fig. 3 and Fig. S8). Whereas the TIM barrel in chain A is intact, with all interstrand hydrogen bonds in place, the TIM barrel in chain B is split into two halves of four strands each (Fig. 3*B*). Comparing the two conformations of the substrate-binding domain to structures of MCM reveals that the closed barrel of chain A resembles the structure of substrate-bound MCM (27, 35), even though no substrate is bound in our holo-IcmF•GDP structure. The open barrel of chain B closely matches the structure of substrate-free MCM (Fig. 3*C*) (23, 27). Thus, chain B, which has the cleaved Cbl cofactor swung out of the active position, also exhibits a disrupted substrate-binding barrel. Although opening and closing of the substrate-binding barrel was previously associated exclusively with substrate binding, here we observe both states in the absence of substrate. The opening is instead accompanied by a displacement of the Cbl out of the active position.

Comparison of Apo- and Holo-IcmF Structures Support Relevance of Domain Motions to G-Protein–Assisted Cofactor Delivery. To investigate the significance of the motion of the Cbl- and G-domains observed in the holo-IcmF•GDP structure, we determined the structure of cofactor-free IcmF (apo-IcmF) to 3.45 Å resolution (Table S1). This structure lacks both AdoCbl and GDP•Mg^{2+} but has the substrate *n*-butyryl-CoA bound. Comparison of the holo and apo structures reveals that the Cbl-binding domain of chain A is no longer tightly associated with its substrate-binding domain. The surface area between these domains has decreased from 1,502 $Å^2$ to 799 $Å^2$, and the Cbl-domain is moved by ∼6 Å from its position in holo-IcmF•GDP (Fig. S9*A*). At the same time, the interface between the Cbl-domain and the G-domain remains intact with an unchanged average buried surface area and no loss of interactions, demonstrating again that the Cbl-domain and the G-domain are moving as one rigid body. This displacement is very similar to that in the holo-IcmF•GDP structure, and as before, it is best described as a swinging motion hinged near the nucleotide-binding site of the G-domain.

Notably, this "open" conformation in apo-IcmF exposes the AdoCbl binding site and the His39-containing loop known to be important for cofactor docking (16) and could therefore depict a structural intermediate in cofactor delivery. To test if this conformation of IcmF is capable of binding AdoCbl, we incubated a preformed apo-IcmF crystal with fresh AdoCbl and determined the resulting structure. Strikingly, the structure reverts back to the active conformation, with AdoCbl bound in the catalytically competent position (Fig. S9 *C* and *D*). Thus, the open conformation is competent for cofactor binding, and cofactor binding triggers a conformational change into the active conformation.

The G-Protein Active Site Undergoes Nucleotide-Sensitive Conformational Changes. The structures of holo-IcmF•GDP and apo-IcmF also allow us to observe changes associated with GDP binding. In the absence of GDP in the apo-IcmF structure, three loops near the G-protein active site are disordered or exhibit conformational changes compared with the holo-IcmF•GDP structure (Fig. S9*B*). These loops include: (*i*) residues 252–256, which immediately precede switch I; (*ii*) residues 312–318, which include the last two residues of switch II and are located next to the residues corresponding to the recently identified switch III region in MeaB (36) (residues 333–344); and (*iii*) residues 281–291, which are packed between loops (*i*) and (*ii*). To examine whether these loop differences are a result of the presence of GDP and not other crystal-to-crystal variations, we incubated a preformed apo-IcmF crystal with GDP•Mg^{2+} and determined the resulting apo-IcmF•GDP structure to 3.25 Å resolution (Table S1). Notably, the loops become ordered (Fig. S9*B*) and adopt the same conformations as observed in the holo-IcmF•GDP structure. Thus, these crystallographic data support the responsiveness to GDP of these three loops in the G protein.

Discussion

G-protein metallochaperones constitute an important enclave of metal homeostasis regulators whose activity in cofactor delivery has been difficult to understand without structural data depicting a metallochaperone:target enzyme complex. The fortuitous fusion of two "stand-alone" proteins into one in IcmF has allowed us to obtain the requisite structural data to interrogate both the signaling pathways and the conformational dynamics related to cofactor delivery. With IcmF serving as a model system, we predict that the human and bacterial MCM:G-protein complexes will form such that their G proteins interact similarly with their mutase domains despite their differences in oligomerization state [bacterial MCM is a heterodimer of an active and an inactive chain (22, 23, 37) and human MCM is a homodimer (33, 38)]. Notably, our structure-based docking model places five pathogenic human mutations—four in human MCM and one in

MMAA—at the MCM:MMAA interface. We now posit that MCM F573S, R616C, G642R, and G648D, as well as MMAA G188R (Table S3) (7), lead to disease because they disrupt the MCM:MMAA interaction, thereby impairing AdoCbl delivery to MCM and causing methylmalonic aciduria. Biochemical data are available to support two of these predictions: the pathogenic G188R mutation in MMAA was shown to inhibit complex formation with human MCM (33) and the pathogenic R616C mutation in MCM was mimicked in a bacterial ortholog and exhibited reduced affinity for MeaB (12).

Our atomic level view of this G-protein:enzyme complex reveals that the switch I region lies at the interface between the G-domain and the Cbl-domain, where it can communicate a signal to regulate Cbl delivery. We have captured multiple structures of both open and closed forms of IcmF and every structure depicts the movement of the Cbl-domain as a concerted displacement of both the Cbl- and the G-domain, with the nucleotide-binding site in the G-domain serving as a hinge. With an interface between the Cbl- and G-domains that appears fairly rigid, the G protein is not just sending a remote signal for the Cbl-domain to move, it is accompanying the Cbl-domain in its movement. Additionally, our structures with and without GDP identify three conformationally flexible loops, which are either near or include residues of the common G-protein elements (switch I and II) and the MeaB/MMAA-specific element known as switch III. Notably, mutations of switch III residues in MeaB affect AdoCbl delivery (36).

Using these structural snapshots and previously published biochemical data (12), we can propose a molecular model for the involvement of G-protein metallochaperones in Cbl delivery (Fig. 4). Enabled by association with the G protein, the Cbl-domain can undergo substantial motions, equilibrating between open and closed conformations. In the open state, the Cbl-domain is partially dissociated from the substrate-binding domain, exposing the His-loop known to be important for cofactor docking (16) and allowing access to the binding pocket for the Cbl dimethylbenzimidazole tail. Indeed, we observe that the open conformation is capable of binding AdoCbl, returning to the catalytically competent closed conformation. AdoCbl delivery (16) should be promoted by GTP binding. Based on the position of GDP, the γ-phosphate of GTP would be positioned between switch I and switch II in a solvent-exposed region, where it could make direct contact with the adenosyltransferase. Alternatively, GTP binding could stabilize the open conformation of the Cbl-domain via the switch I region, but elucidation of the precise role of GTP awaits a GTP-bound structure. In our model, AdoCbl binding and GTP hydrolysis would favor release of the adenosyltransferase and collapse of the open state, sequestering the high value cofactor in its binding pocket. In this catalytically active state, the cofactor is secured by multiple interactions from both the substrate- and Cbl-binding domains, which should inhibit active site reopening and thus prevent inactivation because of loss of the Cbl upper ligand.

In addition to the molecular interactions observed between the G-domain and the Cbl-binding domain that are undoubtedly involved in cofactor delivery, we find that the GTPase active site is located directly at the interface with the mutase substrate-binding domain. This location provides a molecular explanation for the observation that chaperone GTPase activity is affected by binding to a target protein, as observed with MCM:MMAA/MeaB (33, 39). Sizable regions of the GTPase active site are disordered in structures of MeaB and MMAA alone, and likely become ordered upon complex formation to assume the positions observed in IcmF. In particular, complex formation between MCM and MMAA/MeaB is expected to position the conserved Arg (265 in IcmF and 108 in MeaB) at the G-protein:mutase interface such that it can facilitate GTP hydrolysis (Fig. 2*B*). Thus, by the repositioning of a few key side-chains through a protein:protein binding event, communication is established between the substrate-binding domain of the target protein and the GTPase active site of the metallochaperone.

This molecular communication could play a role in mediating conformational changes of the substrate-binding domain that have been observed crystallographically for MCM, with the TIM barrel split open in the absence of substrate and closed in its presence (23, 27). Here, we observe the same open and closed conformations of the TIM barrel, but the correlation is with the absence/presence of Cbl in the barrel as neither structure has substrate. Although the key role of the G-protein metallochaperone must be in AdoCbl loading, MeaB and MMAA also reduce the rate of inactivation of their target enzyme MCM at no cost to catalytic efficiency (6, 18). It is tempting to consider that this protection arises from the G protein assisting conformational changes of the TIM barrel to prevent formation of inactive enzyme states.

In summary, we have provided atomic resolution structures that depict the interaction between an AdoCbl-dependent mutase and its corresponding G-protein chaperone. These structures suggest a molecular pathway to explain the observed bidirectional signaling (12, 36) and indicate how large conformational changes between cofactor- and substrate-binding domains can be achieved to load one of nature's most precious metallocofactors.

Materials and Methods

C. metallidurans icmF was amplified from genomic DNA and ligated into a pET28a vector (Novagen) at the NdeI and BamHI sites. *C. metallidurans* IcmF was purified as described previously (20, 21). IcmF-SeMet was expressed using the methionine biosynthesis inhibition method.

All forms of IcmF were crystallized at 25 °C by hanging-drop vapor diffusion. Purified IcmF at a final concentration of 12 mg/mL was supplemented with 300 μM AdoCbl, 1 mM GDP, and 3 mM $MgCl_2$ to generate holo-IcmF•GDP. For IcmF without AdoCbl and GDP (apo-IcmF), the substrate *n*-butyryl-CoA

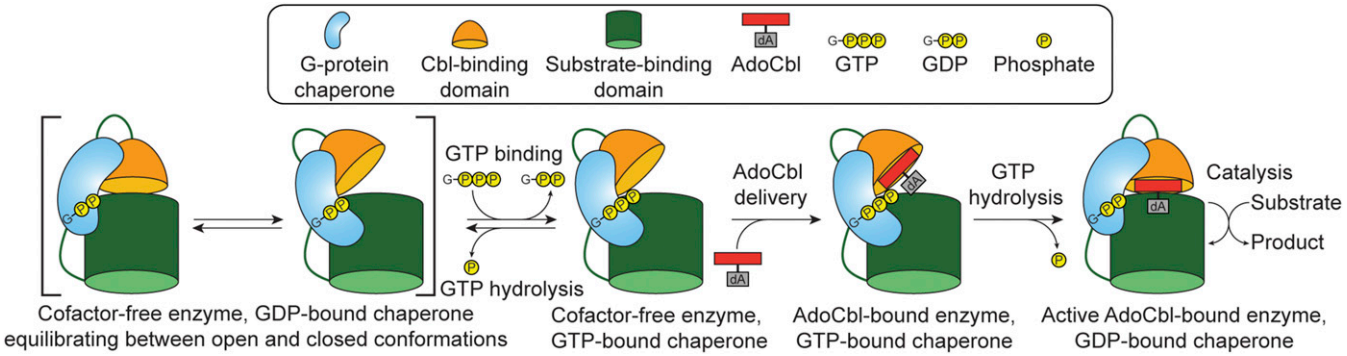

Fig. 4. Schematic of proposed molecular model of Cbl delivery. Only one monomer of the dimer is depicted. See main text for details.

(BCoA, 10 mM) was included to stabilize the protein. To generate crystals of apo-IcmF•GDP, preformed apo-IcmF crystals were soaked with 1 mM GDP and 1.5 mM $MgCl_2$ for 6 h. To reconstitute crystals of apo-IcmF with AdoCbl (apo-IcmF•reconst), preformed apo-IcmF crystals were soaked with 1 mM AdoCbl for 6 h.

All IcmF crystals belong to space group *H*32. A Se anomalous peak dataset for holo-IcmF-SeMet•GDP was collected at the Advanced Light Source (Berkeley, CA) at a wavelength of 0.97914 Å (12663 eV). All other data were collected at the Advanced Photon Source (Argonne, IL). All data were collected at a temperature of 100 K. Data collection statistics are summarized in Table S1.

The holo-IcmF•GDP structure was solved using S/Se-single isomorphous replacement with anomalous scattering, whereas the structures of apo-IcmF, apo-IcmF•GDP, and apo-IcmF•reconst were determined by molecular replacement. The models were refined by iterative cycles of manual adjustment in COOT (40) and refinement in phenix (41). Crystallographic refinement of the structures yielded models that possess low free *R*-factors, excellent stereochemistry, and small rmsd from ideal values for bond lengths and angles. Refinement statistics are summarized in Table S1. Full experimental details are provided in *SI Materials and Methods*.

ACKNOWLEDGMENTS. We thank Yan Kung and Jeremy W. Setser for help with data collection, and Daniel P. Dowling for help with data processing. This work was supported in part by National Institutes of Health Grants GM069857 (to C.L.D.) and DK45776 (to R.B.); and by a Massachusetts Institute of Technology Poitras pre-doctoral Fellowship (to M.J.). C.L.D. is a Howard Hughes Medical Institute Investigator. This work is based in part on research conducted at the Advanced Photon Source on the Northeastern Collaborative Access Team beamlines, which are supported by National Institute of General Medical Sciences Grant P41 GM103403 and the National Institutes of Health. This research used resources of the Advanced Photon Source, a US Department of Energy (DOE) Office of Science User Facility operated for the DOE Office of Science by Argonne National Laboratory under Contract DE-AC02-06CH11357. This work is also based in part on research conducted at the Advanced Light Source, which is supported by the Director, Office of Science, Office of Basic Energy Sciences, of the US Department of Energy under Contract DE-AC02-05CH11231.

1. Tottey S, Harvie DR, Robinson NJ (2005) Understanding how cells allocate metals using metal sensors and metallochaperones. *Acc Chem Res* 38(10):775–783.
2. Finney LA, O'Halloran TV (2003) Transition metal speciation in the cell: Insights from the chemistry of metal ion receptors. *Science* 300(5621):931–936.
3. Robinson NJ, Winge DR (2010) Copper metallochaperones. *Annu Rev Biochem* 79: 537–562.
4. Leipe DD, Wolf YI, Koonin EV, Aravind L (2002) Classification and evolution of P-loop GTPases and related ATPases. *J Mol Biol* 317(1):41–72.
5. Dobson CM, et al. (2002) Identification of the gene responsible for the *cblA* complementation group of vitamin B_{12}-responsive methylmalonic acidemia based on analysis of prokaryotic gene arrangements. *Proc Natl Acad Sci USA* 99(24):15554–15559.
6. Takahashi-Íñiguez T, García-Arellano H, Trujillo-Roldán MA, Flores ME (2011) Protection and reactivation of human methylmalonyl-CoA mutase by MMAA protein. *Biochem Biophys Res Commun* 404(1):443–447.
7. Froese DS, Gravel RA (2010) Genetic disorders of vitamin B_{12} metabolism: Eight complementation groups—Eight genes. *Expert Rev Mol Med* 12:e37.
8. Maier T, Jacobi A, Sauter M, Böck A (1993) The product of the *hypB* gene, which is required for nickel incorporation into hydrogenases, is a novel guanine nucleotide-binding protein. *J Bacteriol* 175(3):630–635.
9. Lee MH, Mulrooney SB, Renner MJ, Markowicz Y, Hausinger RP (1992) *Klebsiella aerogenes* urease gene cluster: Sequence of *ureD* and demonstration that four accessory genes (*ureD*, *ureE*, *ureF*, and *ureG*) are involved in nickel metallocenter biosynthesis. *J Bacteriol* 174(13):4324–4330.
10. Maier T, Lottspeich F, Böck A (1995) GTP hydrolysis by HypB is essential for nickel insertion into hydrogenases of *Escherichia coli*. *Eur J Biochem* 230(1):133–138.
11. Soriano A, Hausinger RP (1999) GTP-dependent activation of urease apoprotein in complex with the UreD, UreF, and UreG accessory proteins. *Proc Natl Acad Sci USA* 96(20):11140–11144.
12. Padovani D, Banerjee R (2009) A G-protein editor gates coenzyme B_{12} loading and is corrupted in methylmalonic aciduria. *Proc Natl Acad Sci USA* 106(51):21567–21572.
13. Banerjee R (2003) Radical carbon skeleton rearrangements: Catalysis by coenzyme B_{12}-dependent mutases. *Chem Rev* 103(6):2083–2094.
14. Halpern J (1985) Mechanisms of coenzyme B_{12}-dependent rearrangements. *Science* 227(4689):869–875.
15. Frey PA (2010) Cobalamin coenzymes in enzymology. *Comprehensive Natural Products II Chemistry and Biology*, eds Mander L, Liu H-W (Elsevier, Oxford), Vol 7, pp 501–546.
16. Padovani D, Labunska T, Palfey BA, Ballou DP, Banerjee R (2008) Adenosyltransferase tailors and delivers coenzyme B_{12}. *Nat Chem Biol* 4(3):194–196.
17. Mera PE, Escalante-Semerena JC (2010) Multiple roles of ATP:cob(I)alamin adenosyltransferases in the conversion of B_{12} to coenzyme B_{12}. *Appl Microbiol Biotechnol* 88(1):41–48.
18. Padovani D, Banerjee R (2006) Assembly and protection of the radical enzyme, methylmalonyl-CoA mutase, by its chaperone. *Biochemistry* 45(30):9300–9306.
19. Toraya T (2014) Cobalamin-dependent dehydratases and a deaminase: Radical catalysis and reactivating chaperones. *Arch Biochem Biophys* 544:40–57.
20. Cracan V, Padovani D, Banerjee R (2010) IcmF is a fusion between the radical B_{12} enzyme isobutyryl-CoA mutase and its G-protein chaperone. *J Biol Chem* 285(1): 655–666.
21. Cracan V, Banerjee R (2012) Novel coenzyme B_{12}-dependent interconversion of isovaleryl-CoA and pivalyl-CoA. *J Biol Chem* 287(6):3723–3732.
22. Cracan V, Banerjee R (2012) Novel $B(_{12})$-dependent acyl-CoA mutases and their biotechnological potential. *Biochemistry* 51(31):6039–6046.
23. Mancia F, et al. (1996) How coenzyme B_{12} radicals are generated: The crystal structure of methylmalonyl-coenzyme A mutase at 2 A resolution. *Structure* 4(3):339–350.
24. Reitzer R, et al. (1999) Glutamate mutase from *Clostridium cochlearium*: The structure of a coenzyme B_{12}-dependent enzyme provides new mechanistic insights. *Structure* 7(8):891–902.
25. Berkovitch F, et al. (2004) A locking mechanism preventing radical damage in the absence of substrate, as revealed by the X-ray structure of lysine 5,6-aminomutase. *Proc Natl Acad Sci USA* 101(45):15870–15875.
26. Dowling DP, Croft AK, Drennan CL (2012) Radical use of Rossmann and TIM barrel architectures for controlling coenzyme B_{12} chemistry. *Annu Rev Biophys* 41(41):403–427.
27. Mancia F, Evans PR (1998) Conformational changes on substrate binding to methylmalonyl CoA mutase and new insights into the free radical mechanism. *Structure* 6(6): 711–720.
28. Gasper R, Meyer S, Gotthardt K, Sirajuddin M, Wittinghofer A (2009) It takes two to tango: Regulation of G proteins by dimerization. *Nat Rev Mol Cell Biol* 10(6):423–429.
29. Hubbard PA, et al. (2007) Crystal structure and mutagenesis of the metallochaperone MeaB: Insight into the causes of methylmalonic aciduria. *J Biol Chem* 282(43): 31308–31316.
30. Gasper R, Scrima A, Wittinghofer A (2006) Structural insights into HypB, a GTP-binding protein that regulates metal binding. *J Biol Chem* 281(37):27492–27502.
31. Fong YH, et al. (2013) Structure of UreG/UreF/UreH complex reveals how urease accessory proteins facilitate maturation of *Helicobacter pylori* urease. *PLoS Biol* 11(10): e1001678.
32. Lofgren M, Koutmos M, Banerjee R (2013) Autoinhibition and signaling by the switch II motif in the G-protein chaperone of a radical B_{12} enzyme. *J Biol Chem* 288(43): 30980–30989.
33. Froese DS, et al. (2010) Structures of the human GTPase MMAA and vitamin B_{12}-dependent methylmalonyl-CoA mutase and insight into their complex formation. *J Biol Chem* 285(49):38204–38213.
34. Schneider TR (2000) Objective comparison of protein structures: Error-scaled difference distance matrices. *Acta Crystallogr D Biol Crystallogr* 56(Pt 6):714–721.
35. Mancia F, Smith GA, Evans PR (1999) Crystal structure of substrate complexes of methylmalonyl-CoA mutase. *Biochemistry* 38(25):7999–8005.
36. Lofgren M, Padovani D, Koutmos M, Banerjee R (2013) A switch III motif relays signaling between a B_{12} enzyme and its G-protein chaperone. *Nat Chem Biol* 9(9): 535–539.
37. Francalanci F, Davis NK, Fuller JQ, Murfitt D, Leadlay PF (1986) The subunit structure of methylmalonyl-CoA mutase from *Propionibacterium shermanii*. *Biochem J* 236(2): 489–494.
38. Jansen R, Kalousek F, Fenton WA, Rosenberg LE, Ledley FD (1989) Cloning of full-length methylmalonyl-CoA mutase from a cDNA library using the polymerase chain reaction. *Genomics* 4(2):198–205.
39. Padovani D, Labunska T, Banerjee R (2006) Energetics of interaction between the G-protein chaperone, MeaB, and B_{12}-dependent methylmalonyl-CoA mutase. *J Biol Chem* 281(26):17838–17844.
40. Emsley P, Lohkamp B, Scott WG, Cowtan K (2010) Features and development of Coot. *Acta Crystallogr D Biol Crystallogr* 66(Pt 4):486–501.
41. Adams PD, et al. (2010) PHENIX: A comprehensive Python-based system for macromolecular structure solution. *Acta Crystallogr D Biol Crystallogr* 66(Pt 2):213–221.